Materiales de Construcción 75 (359)
July-September 2025, e380
ISSN-L: 0465-2746
https://doi.org/10.3989/mc.2025.391024

Waste foundry sand and ground granulated blast furnace slag in self-compacting concrete: rheological characterization and thixotropic behavior

L.M. Abril Moreno[a] ✉, L.E. Zapata Orduz[b].

a. Chemical Engineering Department, Universidad Industrial de Santander, (Bucaramanga, Colombia)
b. Civil Engineering Department, Universidad Industrial de Santander, (Bucaramanga, Colombia)
✉: lina2208133@correo.uis.edu.co

Received 25 July 2024
Accepted 28 January 2025
Available on line 10 March 2026

ABSTRACT: The construction sector seeks to enhance efficiency and reduce Portland cement use due to its environmental impact. Self-compacting concrete (SCC) is a sustainable option as it can incorporate waste materials as substitutes for conventional components. The objective of the research was to analyze the rheological properties of SCC by adding waste foundry sand (WFS) and ground granulated blast furnace slag (GGBFS) as substitutes for fine aggregate and cementitious material, respectively, at a maximum of 60% by weight. Fresh concrete properties were obtained by rheological measurements using a factorial design. The factorial design experiment revealed that the dynamic yield stress decreased with increasing concentrations of WFS particles, while the behavior of adding GGBFS particles was non-linear. The presence of WFS particles was the only factor that had a statistically significant impact on plastic viscosity. The breakdown area method indicates that WFS and their combined effect with GGBFS impact the mixture's thixotropy.

KEY WORDS: Self-compacting concrete; Waste foundry sand; Ground granulated blast furnace slag; Rheological parameters; Thixotropy.

Citation/Citar como: Abril Moreno LM, Zapata Orduz LE. 2025. Waste foundry sand and ground granulated blast furnace slag in self-compacting concrete: rheological characterization and thixotropic behavior. Mater. Construcc. 75(359):e380. https://doi.org/10.3989/mc.2025.391024

RESUMEN: *Arena de fundición y escoria granulada de alto horno en hormigón autocompactante: caracterización reológica y comportamiento tixotrópico.* El sector de la construcción pretende mejorar la eficiencia y minimizar el uso de cemento Portland debido al impacto ambiental. El hormigón autocompactante (SCC), una opción sostenible, puede utilizar materiales de desecho como sustitución de los originales. Esta investigación tuvo como objetivo estudiar el comportamiento reológico del SCC incorporando arena de fundición (WFS) y escoria granulada de alto horno (GGBFS) como reemplazo parcial del árido fino y del cemento hasta un 60% en masa, respectivamente. Las propiedades del hormigón fresco se obtuvieron mediante mediciones reológicas usando un diseño factorial. Este mostró que el esfuerzo de fluencia dinámico disminuyó a medida que aumentó la concentración de partículas WFS, mientras que adicionar partículas GGBFS exhibió un comportamiento no lineal. El único factor que influyó en la viscosidad plástica fue la presencia de partículas WFS. Según el método ruptura, WFS y su efecto combinado con GGBFS impactan la tixotropía de las mezclas.

PALABRAS CLAVE: Hormigón autocompactante; Arena de fundición; Escoria granulada de alto horno; Parámetros reológicos; Tixotropía.

1. INTRODUCTION

For years, civil engineering has played a vital role in developing materials to meet the needs of the construction industry. Concrete is the most produced construction material and the second most used substance worldwide. However, its widespread use has significant environmental repercussions, as it consumes large quantities of freshwater and relies heavily on Ordinary Portland Cement (OPC) as its primary binding agent (1). OPC production is responsible for 5% of global anthropogenic carbon dioxide emissions and is energy-intensive, requiring substantial raw materials (2, 3). Consequently, there is a growing need to develop more sustainable concrete alternatives to reduce the environmental and economic impacts of this material (4).

In response, various by-products and industrial waste materials are being explored as alternatives to prevent the depletion of natural resources (5). Ground granulated blast furnace slag (GGBFS), a by-product of steel manufacturing, is one such material (6, 7). It functions as a hydraulic binder and can replace portions of OPC in concrete, improving properties such as porosity, compressive strength, and workability (8, 9). Additionally, GGBFS enhances the concrete's resistance to sulfate attack while reducing permeability (10, 11).

The overexploitation of river sand for construction purposes has resulted in Environ. Challenges, including erosion, reduced groundwater levels, and ecological disruption (12). Consequently, the subsistence of the construction industry has met limitations due to restrictions on the extraction of sand from rivers (13). Waste foundry sand (WFS) is a by-product of the ferrous and non-ferrous metal casting industries. Globally, several million tons of WFS are produced each year, and their final destination is open dumps, causing an environmental impact (5). Casting sand stored in the heap is classified as hazardous waste because of the high leaching rate of toxic metals from WFS (14). This material is high in silica content and is covered with a thin film of burned carbon, dust, and a residual binder such as bentonite, chemicals, or resins, making it a promising material for use as a partial replacement for fine aggregates in concrete (15).

This project aims to evaluate the rheological properties of self-compacting concrete (SCC) containing WFS as a fine aggregate substitute and GGBFS as a cement replacement. Traditional workability tests used to evaluate fresh-state concrete behavior often provide empirical and subjective data (16). Therefore, rheology, as a science that studies the deformation and flow of matter (17), offers a more scientific approach by providing quantitative data on critical parameters such as plastic viscosity and yield stress. Plastic viscosity measures the material's resistance to flow, while yield stress defines the stress required to initiate flow. This approach allows for a more objective assessment of concrete behavior in its fresh state (18).

Moreover, concrete presents a thixotropic behavior defined as a gradual decrease in viscosity under shear stress, followed by a gradual recovery of the molecular structure when the shear stress is removed (19). When cement particles react with water, a hydrated membrane covers and binds the particles together. These unions (flocs) can be dispersed and re-coagulated when stressed, showing a thixotropic behavior. Studies have shown that after time, the mixture modifies properties such as yield stress, plastic viscosity, thixotropy, and setting time (20, 21).

Although various studies have explored the individual impacts of GGBFS and WFS on concrete properties (22–24), few have investigated their combined effects, particularly concerning rheological and thixotropic behavior. This study aims to fill this gap by providing a comprehensive analysis of self-compacting concrete containing WFS and GGBFS as replacements for fine aggregate and OPC, respectively.

2. MATERIALS AND METHODS

2.1. Concrete materials

The materials were characterized under the parameters established by the American Society of Testing Materials (ASTM): density according to ASTM C188 (25), specific gravity and absorption percentage according to ASTM C136 (26), unit weight according to ASTM C128 (27), and percentage of voids according to ASTM C29 (28). Table 1 presents the physical parameters and Figure 1. shows the size distribution of fine aggregates (FA) and WFS.

The superplasticizer (SP) used was Sika Viscocrete M5, the third generation of polycarboxylates, with a solid content of 43% and density of 1,080 kg/m^3.

Table 1. Physical properties of the materials used in mixed concrete.

Material Property	Ordinary Portland cement type I (OPC)	Ground granulated blast furnace slag (GGBFS)	Fine aggregates (FA)	Waste foundry sand (WFS)	Coarse aggregates (CA)
Density [kg/m³]	2,990	2,780	-	-	-
Fineness modulus (FM)	-	-	2.01	1.74	-
Specific gravity	-	-	2.49	2.46	2.61
Absorption percentage [%Abs]	-	-	1.62	3.13	2.22
Unit weight at saturated surface dry [kg/m³]	-	-	1,350	1,117	1,493
Voids [%]	-	-	42.4	48.8	43.0
Maximum nominal size (MNS) [mm]	-	-	-	-	9.52

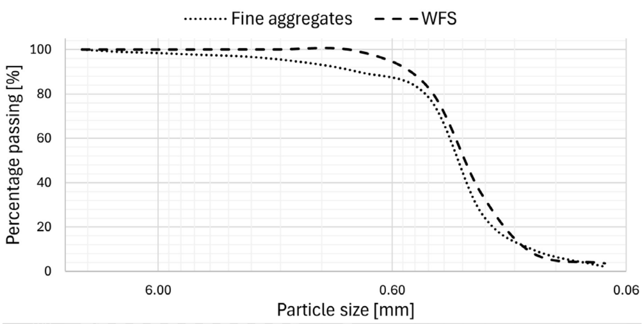

Figure 1. Size distribution curves.

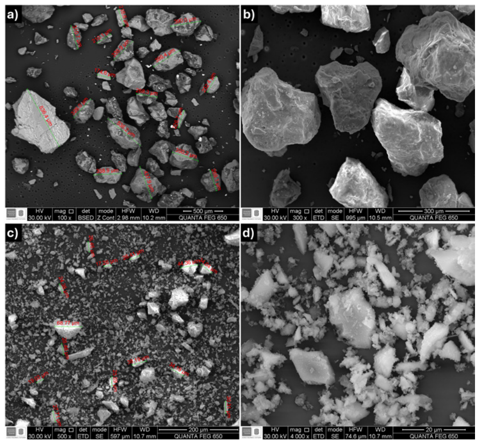

Figure 2. Microestructure of (a) WFS [500 μm] (b) WFS [300 μm] (c) GGBFS [200 μm] (d) GGBFS [20 μm].

2.1.1. Microstructure of GGBFS and WFS

The WFS and GGBFS were microstructurally analyzed using a scanning electron microscope at the UIS scanning electron microscopy laboratory (SEM; QUANTA Field Emission Gun 650), with its operating conditions of high vacuum and accelerating voltage of 30 kV. The samples were placed on metal stubs with carbon adhesive tape and coated with gold to produce a thin conducting film.

According to Figure 2a and Figure 2b, WFS particles vary between angular and subrounded shapes with few edges and smooth angles. They present an average particle size of 300 μm without voids (according to Figure 1 and Figure 2a, 2b). In the case of GGBFS, Figure 2c, 2d shows an agglomeration of particles because of its small particle size. It presents an irregular shape and smooth surface.

2.2. Concrete mix design

The control mix design was developed based on the recommendations for self-compacting concrete (SCC) mixes presented by Okamura et al. (29). For the control mix, designated as GGBFS0-WFS0 (with 0% GGBFS and 0% WFS), the mix proportions from Okamura and Ouchi were followed as closely as possible, considering the available materials. Adjustments were made to the superplasticizer content based on fresh-state tests to ensure the mixture's self-compactness, in accordance with The European Guidelines for Self-Compacting Concrete Specification (EFNARC) (30).

The fresh-state test for the control mix design was the slump flow and T_{500} time test (31). In this test, the average spread diameter of the concrete was measured in two perpendicular directions after the Abrams cone was lifted. According to EFNARC guidelines, the acceptable slump flow range for SCC is between 650 and 800 mm (32). The T_{500} time is the time it takes for the concrete to reach a spread diameter of 500 mm after lifting the cone.

In accordance with EFNARC specifications, SCC performance is confirmed with a flow time between 2 and 5 seconds (32).

The amounts of coarse aggregate (CA), superplasticizer (SP), and the water-to-Cementitious material ratio were kept constant across all mixtures. The solid content of the superplasticizer was maintained at 0.4% of the mass of the cementitious material. Meanwhile, the proportions of GGBFS and WFS in each mixture were calculated based on the mass of the cement and fine aggregates (FA), respectively. Table 2 presents the concrete mix proportions used in the study.

Table 2. Proportions of the raw materials for the concrete mixes.

Mixture	Cement [kg/m^3]	GGBFS [kg/m^3]	FA [kg/m^3]	WFS [kg/m^3]	CA [kg/m^3]	SP [kg/m^3]	Water-to-Cementitious material ratio
GGBFS0-WFS0	536.1	0.0	662.5	0.00	884.8	4.2	0.33
GGBFS0-WFS30	536.1	0.0	463.8	198.8	884.8	4.2	0.33
GGBFS0-WFS60	536.1	0.0	265.0	397.5	884.8	4.2	0.33
GGBFS30-WFS0	375.2	160.8	662.5	0.00	884.8	4.2	0.33
GGBFS30-WFS30	375.2	160.8	463.8	198.8	884.8	4.2	0.33
GGBFS30-WFS60	375.2	160.8	265.0	397.5	884.8	4.2	0.33
GGBFS60-WFS0	214.4	321.6	662.5	0.00	884.8	4.2	0.33
GGBFS60-WFS30	214.4	321.6	463.8	198.8	884.8	4.2	0.33
GGBFS60-WFS60	214.4	321.6	265.0	397.5	884.8	4.2	0.33

2.3. Factorial design

This study was based on a factorial experimental design with two factors, each tested at three levels, along with a central point (3^k design). The factors were the percentage of GGBFS replacing Portland cement and the percentage of WFS replacing fine aggregate. The levels for both factors were set at 0%, 30%, and 60% by mass. Figure 3 presents a schematic representation of the resulting 3^k design. A total of nine combinations were generated, each corresponding to a unique set of factor levels, representing the proportions used in the different concrete mixtures.

An analysis of variance (ANOVA) was performed to analyze the results of the experimental design. ANOVA is a statistical method used to evaluate differences between two or more groups (33). In this analysis, several statistical terms are utilized: degrees of freedom (DF), which define the probability distributions and are determined from the experimental data; sum of squares (SS) and mean squares (MS), which are used to estimate variance; the F-value, which represents a probability distribution that takes into account the chosen statistical hypothesis; and the P-value, which indicates the probability that the null hypothesis is true (33). The closer the P-value is to zero, the higher the likelihood of rejecting the null hypothesis.

Additionally, it is important to clarify that a statistical hypothesis is a statement about the values of population parameters, which can be tested using the information contained in a sample. For the ANOVA, the researchers established a significance level of $\alpha = 0.10$. The central point of the experimental design was conducted with 10 replicates, while the radial points were replicated twice, resulting in 26 independent concrete mixtures.

2.4. Rheological tests

The ICAR RHM-3000 concrete rheometer from the International Center for Aggregate Research (ICAR) was used to measure rheological parameters. The rheometer has a cylindrical container with an internal radius of 143 mm, a depth of 280 mm, and a four-bladed paddle rotating coaxially within, using a 23 L sample. The rheological properties, defined by yield stress and plastic viscosity, depend on factors such as aggregate size, shape, surface area, texture, chemical admixtures, supplementary cementitious materials, and the testing method (16, 34, 35). These parameters are obtained through two tests: the flow curve test and the stress growth test.

The flow curve test determines the relationship between shear stress and shear rate (36). Dynamic yield stress, defined as the stress required to sustain flow, is measured as the shear rate decreases from high to low values (37). In this test, the rheometer speed gradually increased from 0 to 0.500 rps, held for 20 seconds to disrupt any thixotropic structure, and then decreased, with torque recorded at various rotational speeds (each maintained for 5 seconds). Figure 4 shows the equilibrium torque values (Y-axis) plotted against rotational speeds (X-axis), from which the data were used to construct the flow curve.

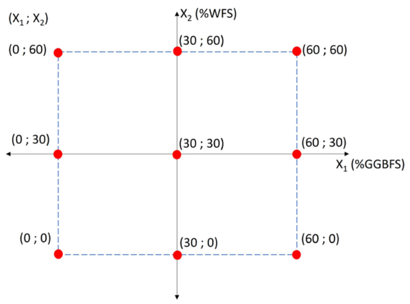

Figure 3. Schematic of the statistical design of experiments.

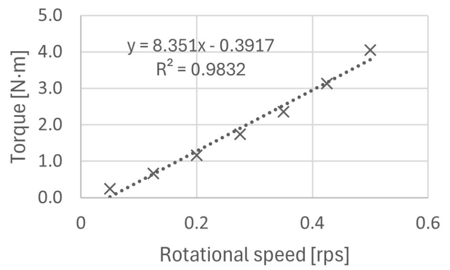

Figure 4. Torque vs. rotational speed for the GGBFS0-WFS30 mix – linear behavior.

The stress growth test involves rotating a four-bladed paddle to induce shear in the concrete at a low, constant speed while measuring the torque. The maximum torque corresponds to the static yield stress, which represents the stress that must be exceeded to initiate flow from a state of rest (37). Figure 5. illustrates a graph showing stress growth. Exceeding this elastic range, the robust connections among cement particles and the attractive forces established during the curing process are disrupted by the maximum stress (19). Upon achieving this maximum stress, the applied shear induces material flow, stopping the increase in torsion value and reaching an equilibrium state known as dynamic yield strength (16).

After conducting the flow curve test, the mixture was left to rest in the container for 5 minutes, and then the structural breakdown test was performed. In this test, the stress growth test was conducted at four different speeds: 0.15, 0.30, 0.45, and 0.60 rps, following the method proposed by Ahari et al. (19). Time-dependent torque measurements were recorded for each speed, resulting in maximum torque (T_m) and equilibrium torque (T_e) values. The sample mix GGBFS0-WFS30 was randomly selected from all the samples under investigation to display the graph (Figure 6).

Subsequently, the initial and equilibrium torque values were graphed against rotational speed, as shown in the example in Figure 7. These curves were fitted to second-order polynomial functions, resulting in correlation coefficients (R^2) greater than 0.99 (not shown here due to space limitations). The region between the maximum torque and equilibrium torque curves is referred to as the "breakdown area" (19). Integration techniques were used to calculate this area, which represents the thixotropy and structural breakdown.

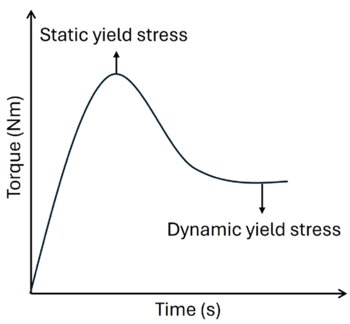

Figure 5. Variation of torque over time. From Jiao et al. (16).

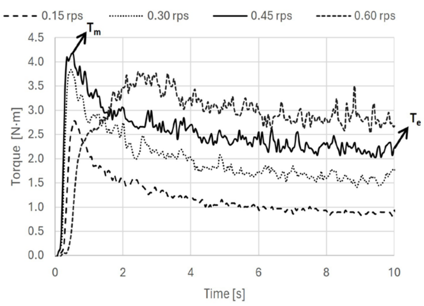

Figure 6. Torque vs. time for the GGBFS0-WFS30 mix.

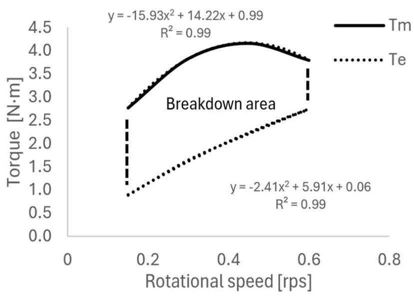

Figure 7. Breakdown area method for mixing for the GGBFS0-WFS30 mix.

3. RESULTS AND DISCUSSION

3.1. Rheological model

The relationship between the values of torque and rotational speed of rheology tests for the experimental points from Figure 3 showed mostly linear behavior, as shown in the example of Figure 4. The linear adjustment of these values for all the mixtures resulted in correlation coefficients (R^2) near 0.98. This linear behavior between the relation of the torque and the rotational speed is analogous to the linear behavior of the shear st stress and the shear rate after reaching the dynamic yield stress, whose slope is the plastic viscosity, corresponding to a Bingham fluid (31, 32) as represented on Equation [1]:

$$\tau = \tau_0 + \mu\dot{\gamma} \qquad [1]$$

where, τ = shear stress [Pa]
τ_0 = dynamic yield stress [Pa]
μ = plastic viscosity [Pa·s]
$\dot{\gamma}$ = hear rate [1/s]

The fit of the data obtained in the rheology tests to the Bingham rheological model was made using the Reiner-Riwlin transformation relations (40, 41) as related in Equation [2] to Equation [4]:

$$T = G + HN \quad [2]$$

$$\tau_0 = \frac{G}{4\pi h}\left(\frac{1}{{R_1}^2} - \frac{1}{{R_2}^2}\right)\frac{1}{Ln\left(\frac{R_2}{R_1}\right)} \quad [3]$$

$$\mu = \frac{H}{8\pi^2 h}\left(\frac{1}{{R_1}^2} - \frac{1}{{R_2}^2}\right) \quad [4]$$

where, T = Torque [N·m]
G = Intercept of the linearization of the results with the Y-axis (see example in Figure 4.) [N·m]
H = Slope of the linearization of the results (see example in Figure 4.) [N·m·s]
N = Rotation speed (see example in Figure 4.) [rps]
R_1 = Rheometer vane radius [mm]
R_2 = Cylindrical container radius [mm]
h = Pallet height [mm]

However, when studying all the rheological curves obtained for the experimental points from Figure 3, with the fit to the Bingham linear model, a deviation of the linear relationship between the shear stress and the shear rate was observed for some of the mixtures, resulting in negative dynamic yield stress values (Table 3).

Table 3. Dynamic yield stress and plastic viscosity results obtained from the Bingham rheological model for the experimental points from Figure 3.

Parameters of the Bingham Rheological Model		
	τ_0 [Pa]	**μ [Pa·s]**
GGBFS0-WFS0	21.10	41.51
GGBFS0-WFS30	8.64	54.06
GGBFS0-WFS60	-0.66	66.28
GGBFS30-WFS0	6.52	46.40
GGBFS30-WFS30	2.88	41.03
GGBFS30-WFS60	-60.19	165.81
GGBFS60-WFS0	10.02	46.33
GGBFS60-WFS30	-23.77	105.44
GGBFS60-WFS60	-25.29	106.76

The negative dynamic yield stress values have no physical explanation and indicate that the previous mathematical adjustment is inadequate to study the behavior obtained in the present tests, owing to the low values of dynamic yield stress (40). To make the adjustment corresponding to this behavior, the modified Bingham model was applied (Equation [5]), which is the Bingham model, but adjusted and expanded to a second-order Taylor polynomial, which considers the non-linearity between the shear stress and the shear rate:

$$\tau = \tau_0 + \mu\dot{\gamma} + c\dot{\gamma}^2 \quad [5]$$

where, τ = shear stress [Pa]
τ_0 = dynamic yield stress [Pa]
μ = plastic viscosity [Pa·s]
$\dot{\gamma}$ = shear rate [1/s]
c = second order parameter [Pa·s^2]

The results obtained from this adjustment were graphically represented and exhibited correlation coefficient values (R^2) of at least 0.99, as shown in Figure 8 for the example mix: GGBFS0-WFS30. Upon obtaining an adequate correlation coefficient, this model was selected for the statistical analysis of the data, discarding other more rigorous mathematical models such as the Herschel-Bulkley model, which is also widely used for SCC.

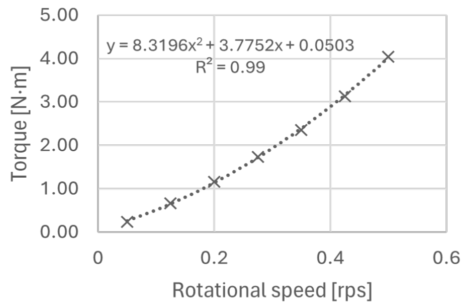

Figure 8. Second-order polynomial behavior between Torque vs. rotational speed (mix: GGBFS0-WFS30).

Table 4. Dynamic yield stress and plastic viscosity of modified Bingham rheological model for the experimental points from Figure 3.

	Parameters of the Modified Bingham Model			
	τ_0 [Pa]	μ [Pa·s]	c [Pa·s²]	c/μ
GGBFS0-WFS0	20.13	42.80	-0.29	-0.007
GGBFS0-WFS30	17.49	42.23	2.64	0.03
GGBFS0-WFS60	8.19	54.44	2.64	0.05
GGBFS30-WFS0	10.34	41.29	1.14	0.06
GGBFS30-WFS30	8.03	32.74	10.85	0.04
GGBFS30-WFS60	7.73	74.96	20.24	0.27
GGBFS60-WFS0	14.48	40.37	1.33	0.03
GGBFS60-WFS30	8.24	62.64	9.54	0.15
GGBFS60-WFS60	5.24	65.92	9.10	0.14

The curves resulting from the fit of all tests to the modified Bingham rheological model were transformed using Reiner-Riwlin's transformation relations (41, 42) as per Equation [6] to Equation [9].

$$\mathrm{T} = G + HN + CN^2 \qquad [6]$$

$$\tau_0 = \frac{G}{4\pi h}\left(\frac{1}{{R_1}^2} - \frac{1}{{R_2}^2}\right)\frac{1}{Ln\left(\frac{R_2}{R_1}\right)} \qquad [7]$$

$$\mu = \frac{H}{8\pi^2 h}\left(\frac{1}{{R_1}^2} - \frac{1}{{R_2}^2}\right) \qquad [8]$$

$$c = \frac{C}{8\pi^2 h}\left(\frac{1}{{R_1}^2} - \frac{1}{{R_2}^2}\right)\left(\frac{R_2 - R_1}{R_2 + R_1}\right) \qquad [9]$$

where, T = torque [N · m]
N = rotation speed [rps]
R_1 = rheometer paddle radius [mm]
R_2 = cylindrical container radius [mm]
h = pallet height [mm]
C, H = parameters obtained from the fit to the second-order polynomial.

After performing the mathematical analysis in the current study, the newly obtained results no longer displayed negative dynamic yield stress values, as indicated in Table 4. The examination of the ratio c/μ elucidates the non-linear behavior. Shear thickening refers to the increase in viscosity caused by shear when the ratio of c/μ is more than 0. Shear thinning, on the other hand, refers to the decrease in viscosity caused by shear when the ratio of c/μ is less than 0. A ratio of c/μ equal to 0 suggests a linear behavior, similar to that of the linear Bingham model (43). The control mix, GGBFS0-WFS0, exhibits a unique "shear thinning" behavior compared to the other mixes due to the absence of WFS and GGBFS. This behavior is characterized by a decrease in viscosity as the shear stress increases. Additionally, it possesses a negative value for c and c/μ. This phenomenon may occur due to the absence of cluster formation in samples containing WFS and GGBFS, which would otherwise produce a reversible rise in viscosity. The lack of cluster formation is attributed to the dominance of repulsive forces over hydrodynamic forces (44, 45).

3.2. Statistical analysis of rheological and thixotropic parameters

Table 5. and Table 6. show the results of the analysis of variance (ANOVA) for the dependent variables: dynamic yield stress and plastic viscosity. The present authors decided to use a significance level of α = 0.10. The results show that GGBFS, WFS, and the interaction of GGBFS▪WFS was statistically significant for the dynamic yield stress (P-values ≤ α-value). On the other hand, only the WFS was significant for the plastic viscosity, indicating that statistically speaking, the presence of GGBFS does not affect the plastic viscosity.

Table 5. Result of the analysis of variance for dynamic yield stress.

Dynamic yield stress (τ_0)					
Factors	DF	Adjusted SS	Adjusted MS	F-value	P-value
GGBFS	1	74.91	74.91	7.45	0.03
WFS	1	230.64	230.64	22.93	0.00
GGBFS▪ GGBFS	1	22.03	22.03	2.19	0.18
WFS▪WFS	1	9.19	9.19	0.91	0.37
GGBFS▪ WFS	1	42.25	42.25	4.2	0.08

Table 6. Result of the analysis of variance for plastic viscosity.

Plastic viscosity (μ)					
Factors	DF	Adjusted SS	Adjusted MS	F-value	P-value
GGBFS	1	3.95	3.95	1.55	0.25
WFS	1	17.72	17.72	6.94	0.03
GGBFS▪ GGBFS	1	0.09	0.09	0.04	0.85
WFS▪WFS	1	3.63	3.63	1.42	0.27
GGBFS▪ WFS	1	0.81	0.81	0.32	0.59

With a significance level of α = 0.10 for the thixotropic parameters obtained using the breakdown area method shows that the presence of GGBFS and the interaction GGBFS▪WFS were statistically significant (Table 7). A slight discrepancy of 1% for the WFS was presented; nevertheless, since the interaction term was important, statistical theory deactivated this variable automatically.

Table 7. Analysis of variance for thixotropic parameters.

Method 1: Breakdown Area					
Factors	DF	Adj SS	Adj SMC	F-value	P-value
GGBFS	1	2.03	2.03	7.64	0.03
WFS	1	0.91	0.91	3.44	0.11
GGBFS▪ GGBFS	1	0.58	0.58	2.2	0.18
WFS▪WFS	1	0.43	0.43	1.63	0.24
GGBFS * WFS	1	1.27	1.27	4.78	0.06

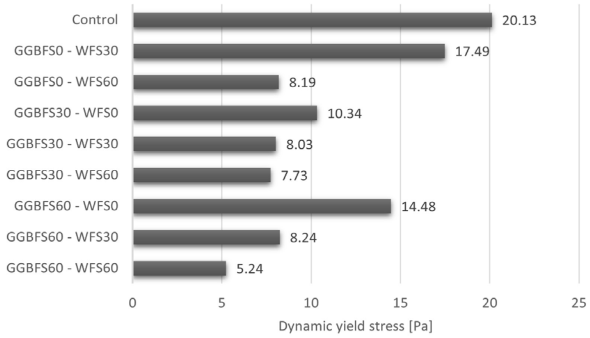

Figure 9. Dynamic yield stress of the experimental mixtures from Figure 3.

3.2.1. Dynamic yield stress

The values obtained for the dynamic yield stress for the experimental points from Figure 3 were graphically recorded in Figure 9. The integration of WFS and GGBFS resulted in a general decrease in the dynamic yield stress compared to the control sample, with reductions ranging from 59% to 73%. Whereas, by using only GGBFS, the reduction was from 28% to 48%, and by using only WFS, the reduction oscillated between 13% to 59%. Recalling that dynamic yield stress is minimum stress required for maintaining flow; it could be deduced that a significant workability improvement is obtained when making SCC with WFS and GGBFS in ranges from 30 – 60% as a replacement by mass. This result is directly applied when the SCC is intended to be used with pumping technologies; for example, mixes such as GGBFS30 – WFS60, GGBFS60 – WFS30, or GGBFS60 – WFS60 could be used. Even using each material alone could reduce the dynamic yield stress, as demonstrated by the ANOVA analysis in Table 5; nevertheless, the combined effect is more effective than using the materials individually.

WFS has a lower fineness modulus and higher absorption capacity to fine aggregates, which suggests the potential for increased particle content in the matrix and improve particle dispersion in the mixture. This leads to increased particle packing of the granular skeleton and reduced global void content (46). Further, reduction in dynamic yield stress can be attributed to the morphology of WFS particles (Figure 2a, 2b), which have subrounded shapes that facilitate movement and avoid interactions between coarse particles.

Adding GGBFS to concrete can reduce dynamic yield stress from 30% addition, with values of 60% being highly effective. However, for values above 60%, an increase in dynamic yield stress was detected, when doing experiments out of the experimental plan here exposed in Figure 3, still the values remained below the control sample of 20.13 [Pa]. This is due to the complex and non-linear behavior of supplementary materials, which cannot be generalized by absolute theories applicable to all cases. The composition of each mix, as well as its interaction with other components, influences the optimal dosage point, thereby affecting the resulting properties of the concrete (47, 48). The decrease in dynamic yield stress may be due to their lower chemical activity and adsorption potential. GGBFS also has a micro-filling effect, influencing rheological properties and generating better matrix dispersity (9). A broad particle size distribution of GGBFS could improve concrete's rheology by increasing free water (49). Adjusting the GGBFS dosage is crucial to avoid an increase in dynamic yield stress due to the non-linear replacement effect.

3.2.2. *Plastic viscosity*

Figure 10. shows the plastic viscosity findings obtained for each mixture. As a result of incorporating WFS, a gradual increase in plastic viscosity was observed. Also, by adding GGBFS without WFS, results like those obtained by the control mixture. The combination of both materials in proportions of at least 30% (by mass) showed a significant increase in plastic viscosity between 8% and 42%. Nevertheless, unlike dynamic yield stress, the ANOVA analyses (Table 6) revealed that the WFS was the only statistically significant modifier variable relative to the plastic viscosity. Therefore, when making SCC, the only presence of WFS in replacement amounts of about 60% (more precisely, higher than 30%) by the fine aggregate mass could guarantee high cohesion and an essential reduction in segregation tendency. In general terms, casting under the same conditions and proportions, the reduction in the tendency could be at least twice when compared with SCC without replacement since the results showed an increase of plastic viscosity of more than 250% when compared with the control mixture (see Figure 10).

As mentioned in section 3.2.1, WFS has a lower fineness modulus and a higher absorption capacity than fine aggregate, which generates an increase in the total surface area. As the total specific surface area (SSA) of a solid increase, the thickness of the suspended liquid covering the solid particles in the concrete mix decreases (46). Consequently, the authors suggest that concrete containing WFS requires more water than other samples to achieve matrix flowability without segregation, increasing the plastic viscosity.

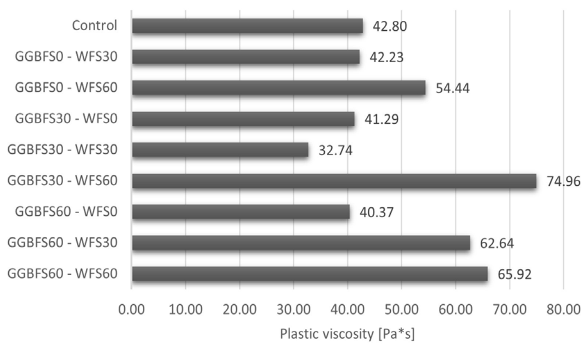

FIGURE 10. Plastic Viscosity of the experimental mixtures from Figure 3.

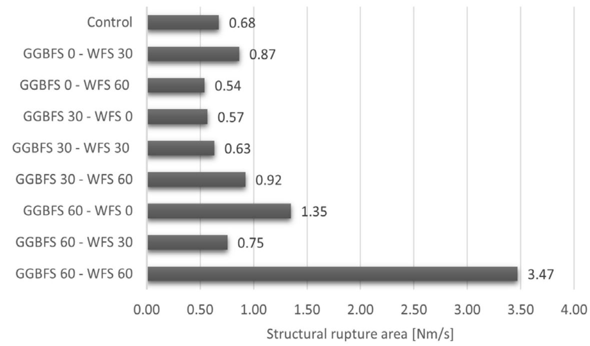

FIGURE 11. The breakdown area method of the experimental mixtures is shown in Figure 3.

3.2.3. *Thixotropic behavior: Breakdown area method.*

As seen in Figure 11 and Table 7, the breakdown area method results are significantly impacted by the addition of GGBFS and the interaction of GGBFS▪WFS. With 60% of GGBFS and 0.0% of WFS, the breakdown area value increased by 98.5% compared to the control sample. Thixotropy and yield stress are dependent on particle packing and colloidal particle interaction, which are responsible for flocculation. When GGBFS is added, finer particles can break Portland cement particles' bonds, filling voids and providing additional lubricant around aggregate particles. This increases packing density and reduces shear stress required to maintain flow (50, 51). However, the breakdown area decreases only up to a specific dosage, exhibiting a non-linear effect. Above this value (60% of GGBFS), the thixotropic behavior is linked to the SSA of the cementitious material used. The finer the material, the greater the SSA, causing increased cohesion and flocculation between particles in the suspension of the cement paste. This results in higher pressures of formwork and fault planes during concrete casting in multiple layers (52).

The interaction between GGBFS and WFS in the mix is statistically significant at a significance level of α = 0.10. The thixotropy behavior of the mix is influenced by the relationship between the initial shear stress and the equilibrium shear stress. When 30% of fine aggregates (FA) are substituted with WFS, there is a noticeable rise in thixotropy values. However, as the replacement level of FA with WFS reached 60%, the thixotropic values experienced a decline. The angular and rounded shape of the WFS may decrease the equilibrium torque values while increasing the difference with the initial torque levels at a given rotating speed. The utilization of WFS and GGBFS can be proven to have a synergistic effect.

4. CONCLUSIONS

The following conclusions can be drawn from the mathematical analysis and the experimental results analyzed statistically by using ANOVA with a significance level of α = 0.10:

- Fitting the data to the linear Bingham rheological model showed a deviation from the relationship between shear stress (τ) and shear rate ($\dot{\gamma}$), resulting in negative yield stress values, which have no physical explanation and represent a thickening of the fresh self-compacting concrete. An adequate adjustment was obtained with the modified Bingham model since it considers the non-linearity of the results and adapts to the thickening of the mix, resulting in positive values of dynamic yield stress with physical meaning and correlation coefficients (R^2) greater than 0.99.
- The dynamic yield stress values changed according to the ANOVA results for both GGBFS and WFS. Adding WFS and GGBFS can reduce the dynamic yield stress according to their morphologies. WFS has a subrounded form that makes it easier to move through it and creates a ball-bearing effect that prevents particle interactions and touch. GGBFS particles, on the other hand, have a smooth surface, less chemical activity, and a micro-filling effect that affects the rheological properties and might result in a more excellent dispersion of the matrix. As a result, there is a notable improvement in workability, which may find utility in areas such as pumping technology.
- According to the ANOVA results, GGBFS had no statistically significant impact on the plastic viscosity; only the presence of WFS was substantial. The plastic viscosity increased after the addition of WFS. Samples with WFS required more water than other samples to provide the matrix fluidity since it has a lower fine modulus, higher absorption capacity, and higher void content than fine aggregate. This behavior could guarantee high cohesion and significantly reduce the segregation tendency in self-compacting concrete mixes.
- The inclusion of GGBFS and their combined effect with WFS impact on the mixtures' thixotropy, according to the method employed to measure it. At a particular concentration (less than 60% of replacement), the presence of GGBGS particles can assist in reducing the shear stress needed to sustain flow by filling in the gaps and adding extra lubricant surrounding aggregates. This helps to break the bindings between Portland cement particles. On the other hand, due to its angular subrounded shape and more significant surface area than fine aggregate, the inclusion of WFS may increase initial torque levels, reducing the equilibrium torque values.

Acknowledge

This research was made possible through the financial support provided by the Vicerrectoría de Investigación y Extensión (VIE) under mobility number 4288 from the Universidad Industrial de Santander (UIS) and the Mater. Struct. Research Group (INME) at the School of Civil Engineering. The authors express their gratitude to Aleisy Bareño Bernal, Diana Montero Parra, and Sergio Ruiz Martínez for their assistance with data collection and management. Lastly, appreciation is given to the UIS Scanning Electron Microscopy Laboratory for conducting the SEM microscopy tests on the samples.

Authorship contribution statement

Luis Eduardo Zapata Orduz: Conceptualization, Funding acquisition, Project administration, Resources, Supervision, Validation, Visualization, Writing-review and editing.

Lina María Abril Moreno: Data curation, Formal analysis, Investigation, Methodology, Software, Visualization, Writing-original draft, Writing-review and editing.

Declaration of competing interest

The authors of this article declare that they have no financial, professional or personal conflicts of in-terest that could have inappropriately influenced this work.

REFERENCES

1. Adesina A. 2020. Recent Advances in the concrete industry to reduce its carbon dioxide emissions. Environ. Challenges. 1:100004. https://doi.org/10.1016/j.envc.2020.100004
2. Andrew RM. 2018. Global CO2 emissions from cement production. Earth Syst. Sci. Data. 10(1):195–217. https://doi.org/10.5194/essd-10-195-2018
3. He Z, Zhu X, Wang J, Mu Mulan, Wang Y. 2019. Comparison of CO_2 emissions from OPC and recycled cement production. Constr. Build. Mater. 211:965–973. https://doi.org/10.1016/j.conbuildmat.2019.03.289
4. Di Filippo J, Karpman J, DeShazo JR. 2019. The impacts of policies to reduce CO2 emissions within the concrete supply chain. Cem. Concr. Compos. 101:67–82. https://doi.org/10.1016/j.cemconcomp.2018.08.003
5. Bhargav Kumar KP, Krishna G, Umashankar B. 2019. Evaluation of waste foundry sand and blast furnace steel slag as geomaterials. Geo-Congress 2019: Geoenvironmental Engineering and Sustainability (GSP 312), 304–313. https://doi.org/10.1061/9780784482148.031
6. Senani, M, Ferhoune N, Guettala A, Aguiar JB. 2018. Eco-Concrete with incorporation of blast furnace slag as natural aggregates replacement. Sci. Technol. Mater. 30(3):144–50. https://doi.org/10.1016/j.stmat.2017.12.001
7. Tavasoli S, Nili M, Serpoosh B. 2018. Effect of GGBS on the frost resistance of self-consolidating concrete. Constr. Build. Mater. 165:717–722. https://doi.org/10.1016/j.conbuildmat.2018.01.027
8. Liu G, Florea MVA, Brouwers HJH. 2019. Characterization and performance of high volume recycled waste glass and ground granulated blast furnace slag or fly ash blended mortars. J. Clean. Prod. 235:461–472. https://doi.org/10.1016/j.jclepro.2019.06.334
9. Isa Y. 2018. 12 - Blast-furnace slag, Editor(s): Rafat Siddique, Paulo Cachim. In Woodhead Publishing Series in Civil and Structural Engineering, Waste and Supplementary Cementitious Materials in Concrete, Woodhead Publishing, 361-415,. https://doi.org/10.1016/B978-0-08-102156-9.00012-2
10. Singh G, Siddique R. 2016. Effect of iron slag as partial replacement of fine aggregates on the durability characteristics of self-compacting concrete. Constr. Build. Mater. 128:88–95. http://doi.org/10.1016/j.conbuildmat.2016.10.074
11. Hadjsadok A, Kenai S, Courard L. 2012. Durability of mortar and concretes containing slag with low hydraulic activity. Cem. Concr. Compos. 34(5):671–677. http://doi.org/10.1016/j.cemconcomp.2012.02.011
12. Sankh AC, Biradar PM, Naghathan SJ, Ishwargol MB. 2014. Recent trends in replacement of natural sand with different alternatives. IOSR Journal of Mechanical and Civil Engineering (IOSR-JMCE), 1:59–66. Retrieved from https://www.iosrjournals.org/iosr-jmce/papers/ICAET-2014/ce/volume-1/10.pdf
13. Bhardwaj B, Kumar P. 2017. Waste foundry sand in concrete:a review. Constr. Build. Mater. 156:661–674. http://doi.org/10.1016/j.conbuildmat.2017.09.010
14. Sawai H, Rahman IMM, Fujita M, Jii N, Wakabayashi T, Begum ZA, Maki T, Mizutani S, Hasegawa H. 2016. Decontamination of metal-contaminated waste foundry sands using an EDTA-NaOH-NH_3 washing solution. Chem. Eng. J. 296:199–208. http://doi.org/10.1016/j.cej.2016.03.078
15. De Barros Martins MA, Mambeli Barros R, Silva G, Silva dos Santos IF. 2019. Study on waste foundry exhaust sand , wfes , as a partial substitute of fi ne aggregates in conventional concrete. Sustain. Cities Soc. 45:187–196. https://doi.org/10.1016/j.scs.2018.11.017
16. Jiao D, Shi C, Yuan Q, An X, Liu Y, Li H. 2017. Effect of constituents on rheological properties of fresh concrete-a review. Cem. Concr. Compos. 83:146–159. http://doi.org/10.1016/j.cemconcomp.2017.07.016
17. Abraham J, Sharika T, Mishra RK, Thomas S. 2017. Rheological characteristics of nanomaterials and nanocomposites. Micro and Nano Fibrillar Composites (MFCs and NFCs) from Polymer Blends, Elsevier Ltd, 2017:327-350. http://doi.org/10.1016/B978-0-08-101991-7.00014-5
18. Faleschini F, Jiménez C, Barra M, Aponte D, Vázquez E, Pellegrino C. 2014. Rheology of fresh concretes with recycled aggregates. Constr. Build. Mater. 73:407–416. https://doi.org/10.1016/j.conbuildmat.2014.09.068
19. Ahari RS, Erdem TK, Ramyar K. 2015. Thixotropy and structural breakdown properties of self consolidating concrete containing various supplementary cementitious materials. Cem. Concr. Compos. 59:26–37. http://doi.org/10.1016/j.cemconcomp.2015.03.009
20. Kala K, Subramaniam KVL. 2022. Alkali-Activated fly ash-blast furnace slag blend rheology:evaluation of yield and maxwell responses. Clean. Eng. Technol. 6:100398. https://doi.org/10.1016/j.clet.2022.100398
21. Güneyisi E, Gesoglu M, Naji N, Ipek S. 2016. Evaluation of the rheological behavior of fresh self-compacting rubberized concrete by using the herschel-bulkley and modified bingham models. Arch. Civ. Mech. Eng. 16(1):9–19. http://doi.org/10.1016/j.acme.2015.09.003
22. Boukendakdji O, Kadri EH, Kenai S. 2012. Effects of granulated blast furnace slag and superplasticizer type on the fresh properties and compressive strength of self-compacting concrete. Cem. Concr. Compos. 34(4):583–590. http://doi.org/10.1016/j.cemconcomp.2011.08.013

23. Ashish DK , Surender KV. 2021. Robustness of self-compacting concrete containing waste foundry sand and metakaolin:a sustainable approach. J. Hazard. Mater. 401:123329. https://doi.org/10.1016/j.jhazmat.2020.123329
24. Tittarelli F. 2018. Waste Foundry Sand. In Waste and supplementary cementitious materials in concrete, Elsevier Ltd, 121–47. https://doi.org/10.1016/B978-0-08-102156-9.00004-3
25. American Society for Testing & Materials. 2023a. Annual Book of ASTM Standards ASTM C188-23: Standard test method for density of hydraulic cement.
26. American Society for Testing & Materials. 2019. Annual Book of ASTM Standards ASTM C136-19: Standard test method for sieve analysis of fine and coarse aggregates.
27. American Society for Testing & Materials. 2022. Annual book of ASTM standards ASTM C128-22: Standard Test method for relative density (specific gravity) and absorption of fine relative density (specific gravity) and absorption of fine aggregate aggregate.
28. American Society for Testing & Materials. 2023b. Annual Book of ASTM Standards ASTM C29-23: Standard test method for bulk density ("unit weight") and voids in aggregate.
29. Okamura H, Ouchi M. 1998. Self-compacting high performance concrete. Prog. Struct. Eng. Mater. 6(4):378–383. http://doi.org/10.2749/101686696780496292
30. EFNARC. 2005. The european guidelines for self compacting concrete the european guidelines for self-compacting concrete:specification, production and use.
31. Ctn, Technical Committee. 2020. Testing fresh concrete part 8 : self-compacting concrete slump-flow test.
32. EFNARC. 2002. 44 Report from EFNARC Specification and guidelines for self-compacting concrete.
33. Montgomery DC. 2013. Design and analysis of experiments. 8th Edition. John Wiley & Sonc, Inc.
34. Bentz DP, Ferraris CF, Galler MA, Hansen AS, Guynn JM. 2012. Influence of particle size distributions on yield stress and viscosity of cement-fly ash pastes. Cem. Concr. Res. 42(2):404–409. http://doi.org/10.1016/j.cemconres.2011.11.006
35. Wallevik JE. 2006. Relationship between the bingham parameters and slump. Cem. Concr. Res. 36(7):1214–1221. http://doi.org/10.1016/j.cemconres.2006.03.001
36. Germann Instruments A/S. 2024. Rheology using the ICAR Plus – An introduction. Retrieved from https://www.germanninstruments.com/concrete-rheometer-icar-plus/ (September 5, 2024)
37. Qian Y, Kawashima S. 2018. Distinguishing dynamic and static yield stress of fresh cement mortars through thixotropy. Cem. Concr. Compos. 86:288–296. https://doi.org/10.1016/j.cemconcomp.2017.11.019
38. Ferraris CF. 1999. Measurement of the rheological properties of high performance concrete: state of the art report. J. Res. Nist. Inst. Stand. Technol. 104(5):18. Retrieved from http://www.nist.gov/jres
39. Campos RS, Maciel GF. 2021. Test Protocol and rheological model influence on determining the rheological properties of cement pastes. J. Build. Eng. 44:103206. https://doi.org/10.1016/j.jobe.2021.103206
40. Feys D, Verhoeven R, De Schutter G. 2008. Fresh self compacting concrete, a shear thickening material. Cem. Concr. Res. 38(7):920–929. http://doi.org/10.1016/j.cemconres.2008.02.008
41. Singh R, Singh B. 2018. Rheological behaviour of different grades of self-compacting concrete containing recycled aggregates. Constr. Build. Mater. 161:354–364. https://doi.org/10.1016/j.conbuildmat.2017.11.118
42. Feys D, Wallevik JE, Yahia A, Khayat KH, Wallevik OH. 2013. Extension of the Reiner-Riwlin equation to determine modified bingham parameters measured in coaxial cylinders rheometers. Mater. Struct./Materiaux et Constructions 46:289–311. http://doi.org/10.1617/s11527-012-9902-6
43. Feys D, Verhoeven R, De Schutter G. 2007. Evaluation of time independent rheological models applicable to fresh self-compacting concrete. Appl. Rheol. 17(5): 56244-1-56244-10. https://doi.org/10.1515/arh-2007-0018
44. Feys D, Verhoeven R, De Schutter G. 2009. Why is fresh self-compacting concrete shear thickening?. Cem. Concr. Res. 39(6):510–523. http://doi.org/10.1016/j.cemconres.2009.03.004
45. Maranzano BJ, Wagner NJ. 2001. The effects of particle size on reversible shear thickening of concentrated colloidal dispersions. J. Chem. Phys. 114: 10514–10527. http://doi.org/10.1063/1.1373687
46. Vance K, Kumar A, Sant G, Neithalath N. 2013. The rheological properties of ternary binders containing portland cement, limestone, and metakaolin or fly ash. Cem. Concr. Res. 52:196–207. http://doi.org/10.1016/j.cemconres.2013.07.007
47. Li Z, Lu D, Gao X. 2020. Multi-objective optimization of gap-graded cement paste blended with supplementary cementitious materials using response surface methodology. Constr. Build. Mater. 248:118552. https://doi.org/10.1016/j.conbuildmat.2020.118552
48. Ongpeng JM, Clemente SJ, Ong CG, Te DD, Tecson JV, Roxas CL. 2022. Influence of supplementary cementitious materials in the concrete's compressive strength through artificial neural network. 2nd International Conference on Civil and Environmental Engineering (ICCEE 2022). E3S Web of Conferences. 347:02004. https://doi.org/10.1051/e3sconf/202234702004
49. Divsholi BS, Darren Lim TY, Teng S. 2014. Durability properties and microstructure of ground granulated blast furnace slag cement concrete. Int. J. Concr. Struct. Mater. 8:157–64. http://doi.org/10.1007/s40069-013-0063-y
50. Assaad J, Khayat KH, Mesbah H. 2003. Assessment of thixotropy of flowable and self-consolidating concrete. ACI Mater. J. 100(2):99–107. http://doi.org/10.14359/12548

51. Dai X, Ren Q, Aydin S, Yardimi MY, Lesage K, De Schutter G. 2021. Enhancing thixotropy and structural build-up of alkali-activated slag/fly ash pastes with nano clay. Mater. Struct./Materiaux et Constructions 54:163. https://doi.org/10.1617/s11527-021-01760-4
52. Roussel N. 2006. A Thixotropy model for fresh fluid concretes :theory , validation and applications. Cem. Concr. Res. 36(10):1797–1806. http://doi.org/10.1016/j.cemconres.2006.05.025